Search for Higgs Boson Pair Production in the $b\bar{b}\tau^+\tau^-$ Final State with the ATLAS Detector

Christopher Deutsch

November 24, 2021

University of Bonn

Higgs Boson Pair Production

Non-Resonant Production

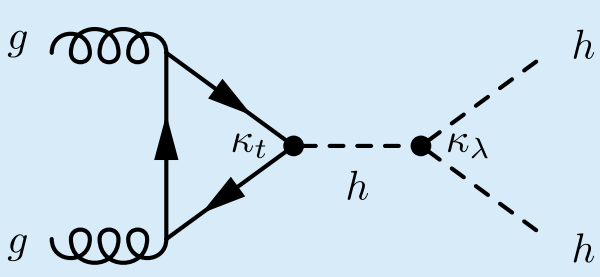

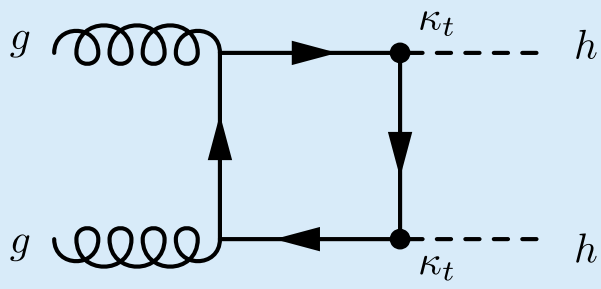

Resonant Production

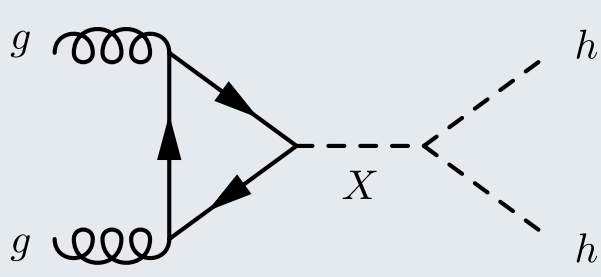

- Direct measurement of self-coupling κ_λ $\rightarrow$ access to Higgs potential
- Small cross section $\sigma_{HH}^{\text{ggF}} = 31.05\,\text{fb}$ * in SM due to destructive interference
  - VBF contribution $\sigma_{HH}^{\text{VBF}} = 1.726\,\text{fb}$ † also considered

- Resonant enhancement in BSM scenarios
- Benchmark model:

  Narrow-width CP-even scalar X

  $251\,\text{GeV} \leq m_X \leq 1.6\,\text{TeV}$

*: NNLO QCD, $m_h = 125$ GeV, pp @ 13 TeV, J. High Energ. Phys. **2018**, 59 (2018)

†: N^{3}LO QCD, $m_h = 125$ GeV, pp @ 13 TeV, Phys. Rev. D **98**, 114016

The $b\bar{b}\tau^+\tau^-$ Final State

Di-Higgs Branching Ratios

	$b\bar{b}$	W^+W^-	$\tau^+\tau^-$	ZZ^*	$\gamma\gamma$
$b\bar{b}$	34 %				
W^+W^-	25 %	4.6 %			
$\tau^+\tau^-$	**7.3 %**	2.7 %	0.39 %		
ZZ^*	3.1 %	1.1 %	0.33 %	0.069 %	
$\gamma\gamma$	0.26 %	0.097 %	0.028 %	0.012 %	0.00052 %

BR for $m_h = 125$ GeV from LHCHXSWG

Di-Tau Branching Ratios

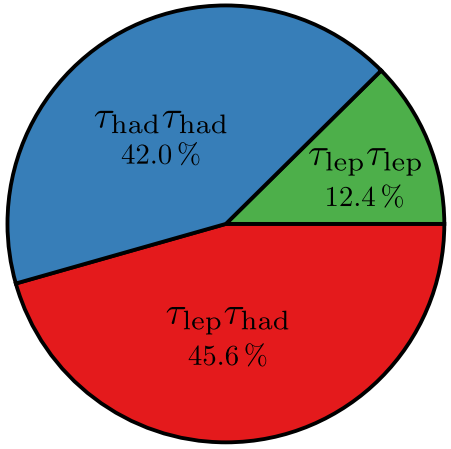

BR from PDG

- $HH \to b\bar{b}\tau^+\tau^-$ third largest BR of relevant channels
- High sensitivity to SM Higgs pair production
- Targeting semi-leptonic ($\tau_{lep}\tau_{had}$) and fully hadronic ($\tau_{had}\tau_{had}$) di-tau final states

Event Selection

$\tau_{had}\tau_{had}$	$\tau_{lep}\tau_{had}$ (SLT)	$\tau_{lep}\tau_{had}$ (LTT)
single & di-τ_{had} triggers	single ℓ triggers	$\ell + \tau_{had}$ triggers
exactly two τ_{had}	exactly one τ_{had} & one e or μ	
lepton-veto	$m_{bb} < 150$ GeV	
trigger-dependent thresholds on $e/\mu/\tau_{had}$ and jets		
$m_{\tau\tau}^{MMC} > 60$ GeV		
2 b-tagged jets		
OS el. charge of $\tau_e/\tau_\mu/\tau_{had}$ and τ_{had}		

Acceptance of non-res. HH (SM):

Channel	$(\mathcal{A} \times \varepsilon)^{\text{ggF+VBF}}_{\text{SM } HH}$
$\tau_{had}\tau_{had}$	4 %
$\tau_{lep}\tau_{had}$ (SLT)	4 %
$\tau_{lep}\tau_{had}$ (LTT)	1 %

ATLAS-CONF-2021-030

ATLAS-CONF-2021-030

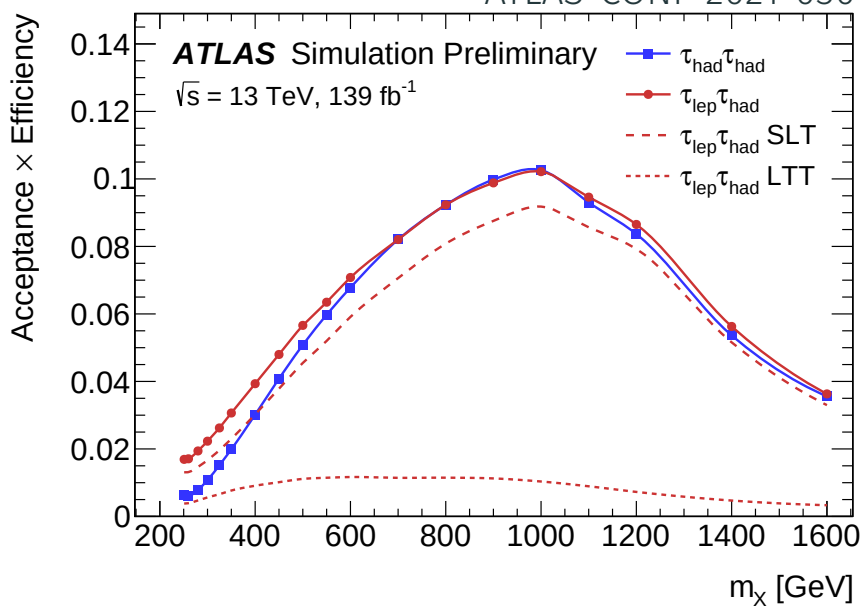

Event Selection

sin

- Close to two-fold improvement in signal acceptance compared to previous publication

  (Phys. Rev. Lett. **121**, 191801)

- Driven by improved reconstruction and identification of τ_{had} and b-jets

  (ATL-PHYS-PUB-2017-003, ATL-PHYS-PUB-2017-013, ATL-PHYS-PUB-2019-033)

Acceptance of non-res. HH (SM):

Channel	$(\mathcal{A} \times \varepsilon)^{\text{ggF+VBF}}_{\text{SM } HH}$
$\tau_{\text{had}}\tau_{\text{had}}$	4 %
$\tau_{\text{lep}}\tau_{\text{had}}$ (SLT)	4 %
$\tau_{\text{lep}}\tau_{\text{had}}$ (LTT)	1 %

ATLAS-CONF-2021-030

ATLAS-CONF-2021-030

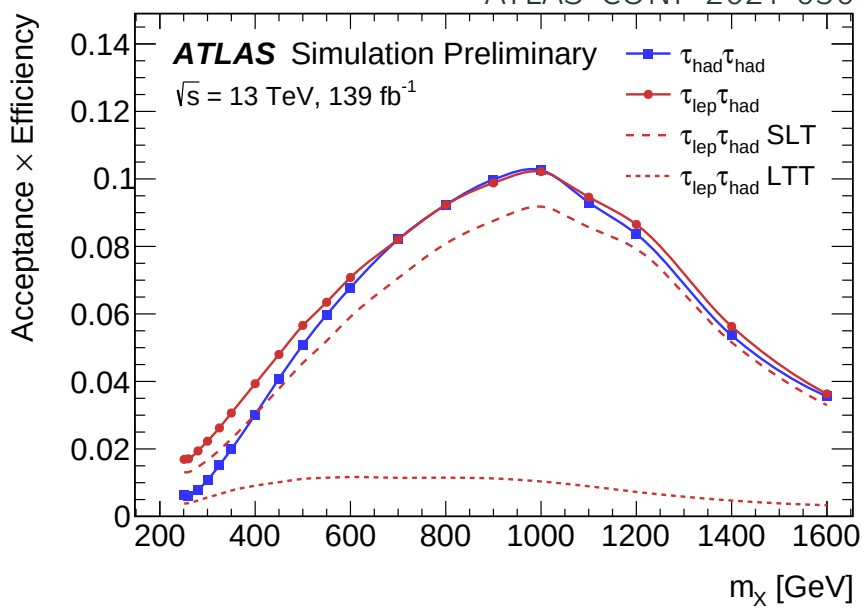

Object Selection Improvements: $\tau_{\text{had-vis}}$ Identification

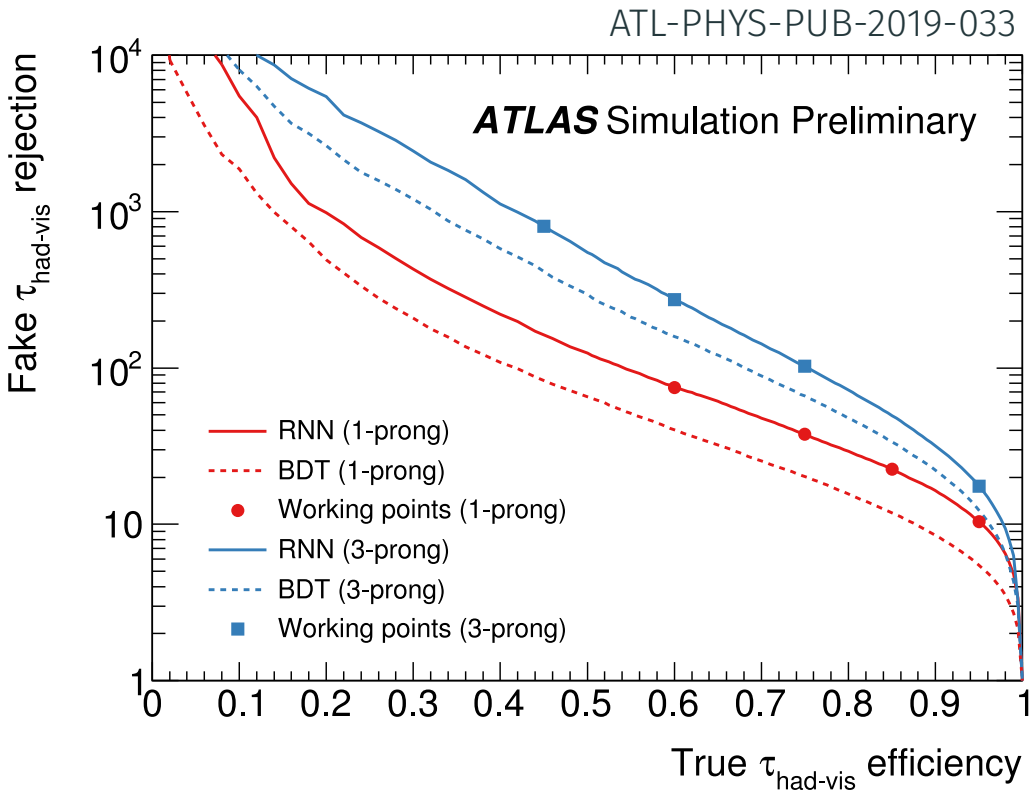

- Moving to "deep learning"-based $\tau_{\text{had-vis}}$-tagging
  - Recurrent Neural Networks operating on sequences of tracks & calorimeter clusters

Object Selection Improvements: $\tau_{\text{had-vis}}$ Identification

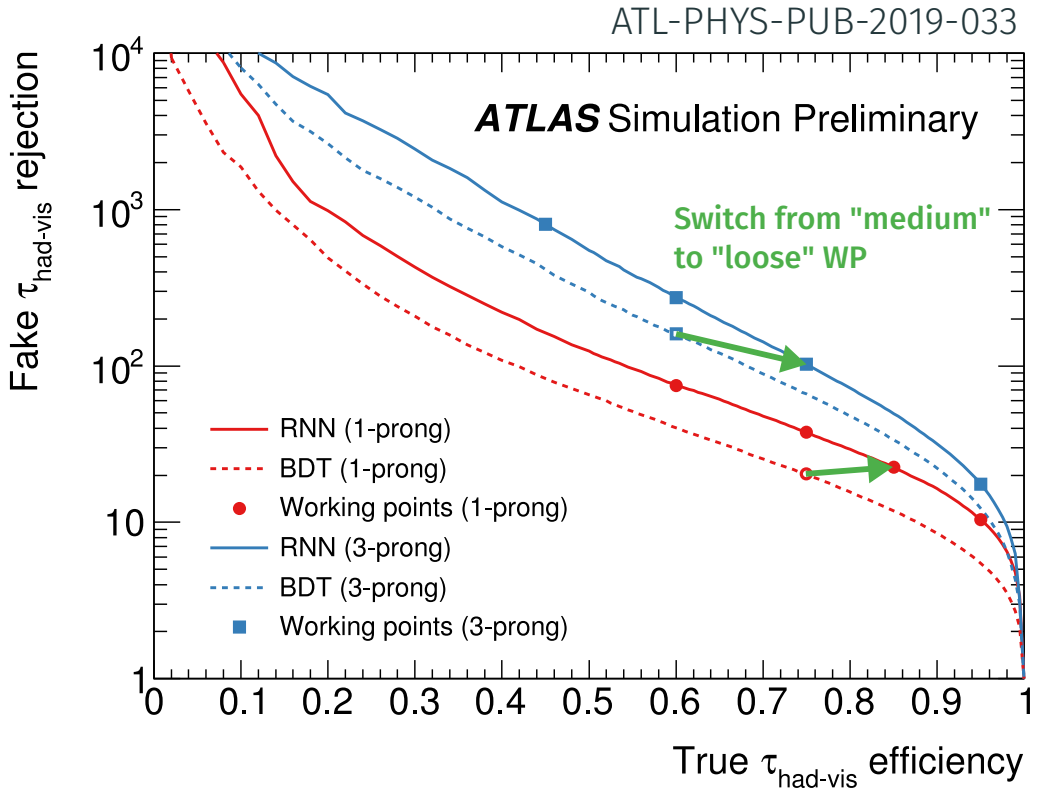

- Moving to "deep learning"-based $\tau_{\text{had-vis}}$-tagging
  - Recurrent Neural Networks operating on sequences of tracks & calorimeter clusters
- Switch from medium to loose τ_{had} WP with similar fake $\tau_{\text{had-vis}}$ rates
  - Particularly beneficial in $\tau_{\text{had}}\tau_{\text{had}}$

Background Estimation

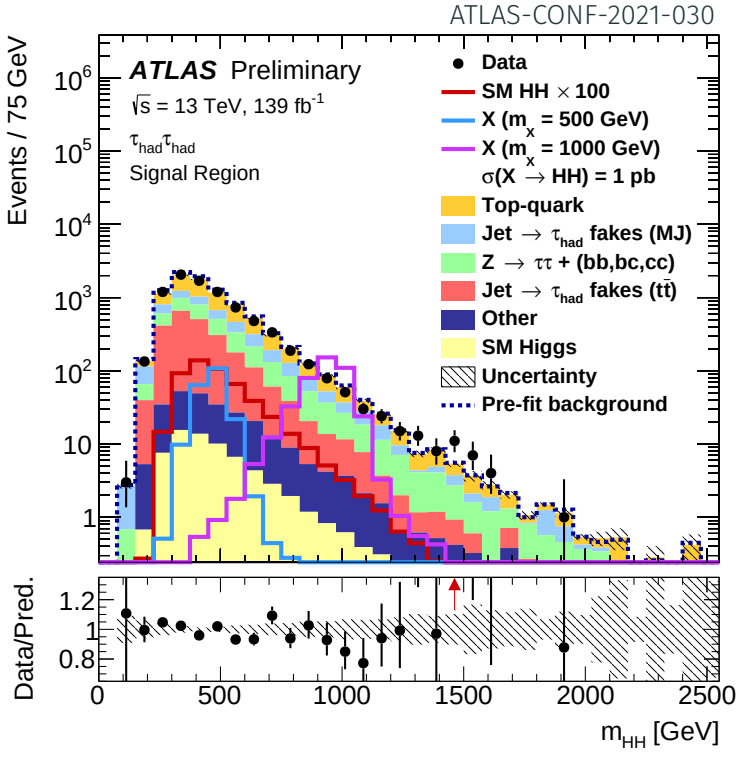

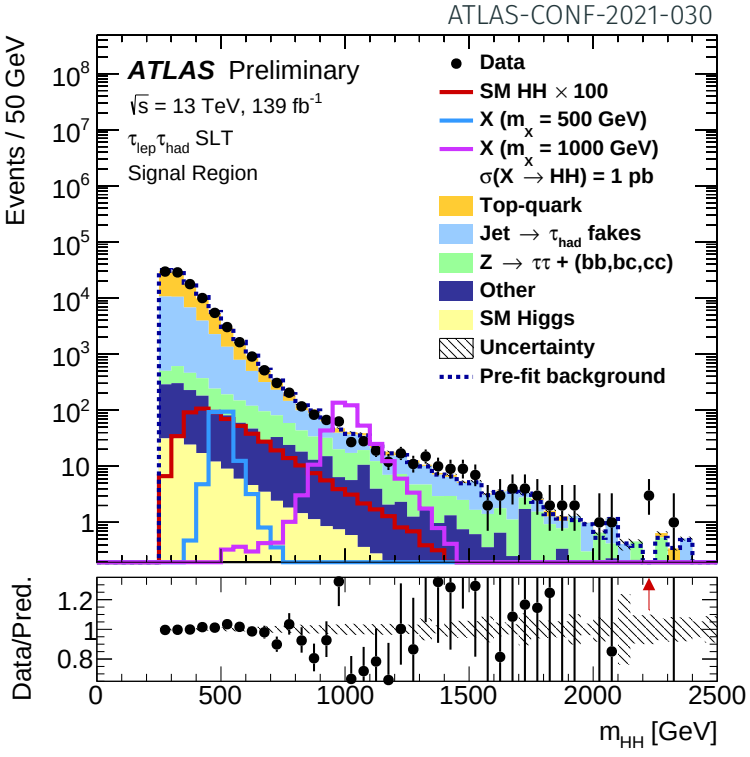

Background	$\tau_{had}\tau_{had}$-channel	$\tau_{lep}\tau_{had}$-channel
$t\bar{t}$	Simulation (normalized in fit)	
Z+jets	Simulation (normalized in fit – dedicated CR)	
jet → τ_{had} fakes ($t\bar{t}$)	Simulation (data-driven mis-ID eff.)	Combined fake-factor method
jet → τ_{had} fakes (multi-jet)	Fake-factor method	
SM Higgs / Other	Simulation	

Background Estimation: Z + Heavy Flavor Jets

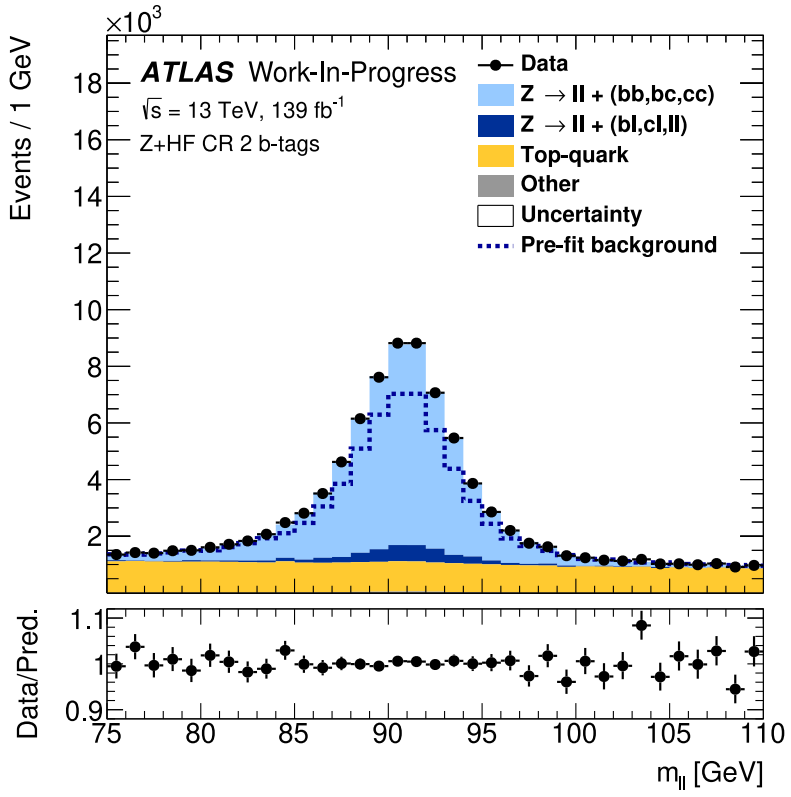

- Normalization discrepancy for Z + heavy flavor jets in Sherpa 2.2.1
- Corrected in fit of $m_{\ell\ell}$ distribution in Z($\rightarrow ee$ / $\mu\mu$) + HF control region

  2 b-tags $\quad m_{\ell\ell} \in [75\,\text{GeV}, 110\,\text{GeV}] \quad m_{bb} \notin [40\,\text{GeV}, 210\,\text{GeV}]$

Background Estimates ($\tau_{had}\tau_{had}$): Multi-Jet $\rightarrow$ τ_{had} Fakes

Fake Factor method:

- Fake Factor (FF) derived in fake-enriched same-sign el. charge τ_{had} region (SS)
- Compare: Events passing τ_{had}-ID to events where one τ_{had} fails ID

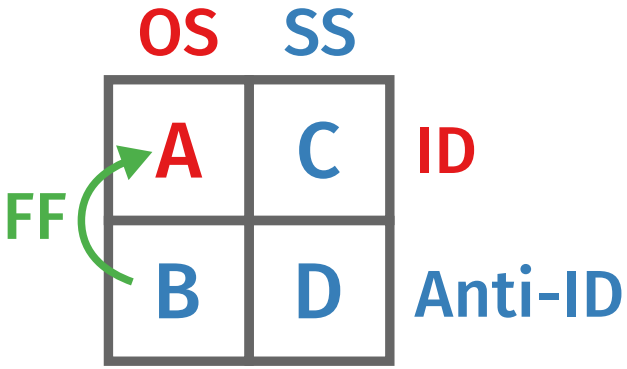

$$\mathrm{FF} = \frac{N_{\mathrm{C}}}{N_{\mathrm{D}}}$$

$$N_{\mathrm{A}} = \mathrm{FF} \cdot N_{\mathrm{B}}$$

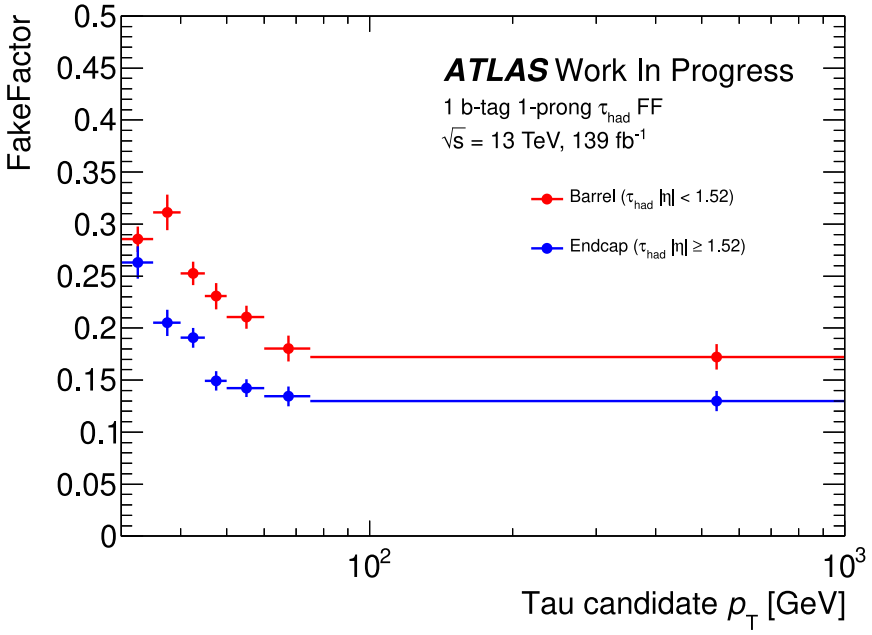

- Fake factors extrapolated from 1 to 2 b-tag region
- Parametrized in: trigger, leading / subleading τ_{had} failing ID, $\tau_{had\text{-}vis}$ p_T / η, τ_{had} prong

Background Estimates ($\tau_{had}\tau_{had}$): Jet $\rightarrow \tau_{had}$ Fakes ($t\bar{t}$)

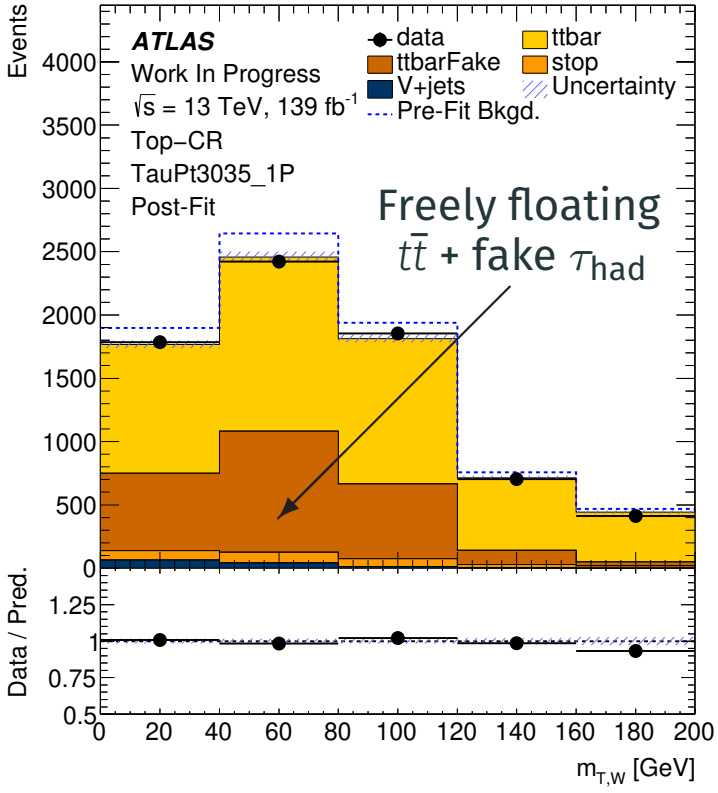

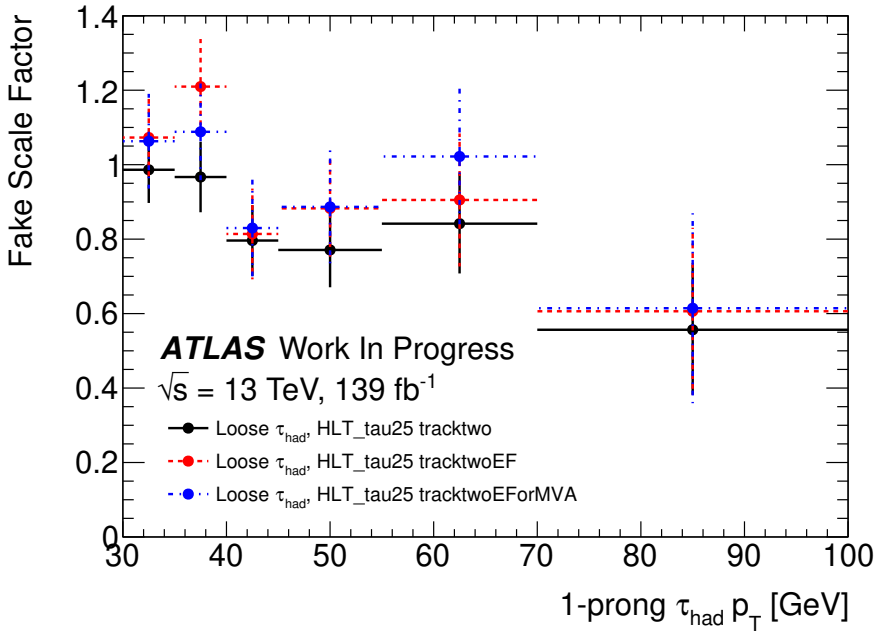

- 40 % of $t\bar{t}$ contains at least one τ_{had} faked by jets
- Measure misidentification efficiency in $t\bar{t}$ enriched 1-lepton + τ_{had} region
  - Shape-fit in $m_{T,W}$ in bins of τ_{had} p_T and prong
  - Accounting for varying HLT τ_{had}-identification throughout Run 2

Signal Extraction: Non-Resonant Higgs Pair Production

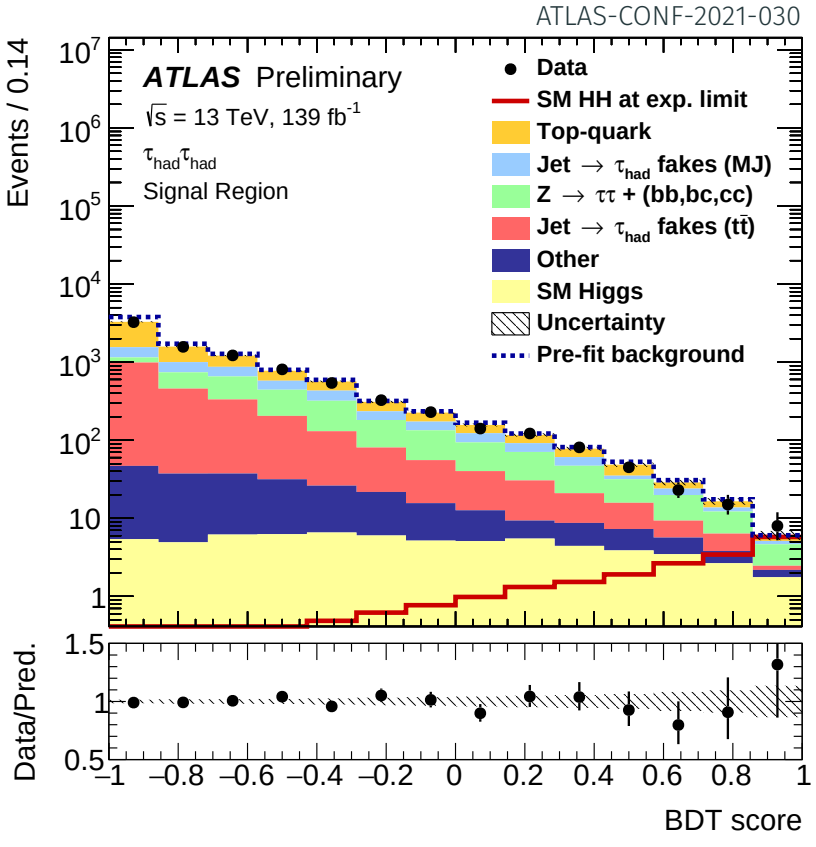

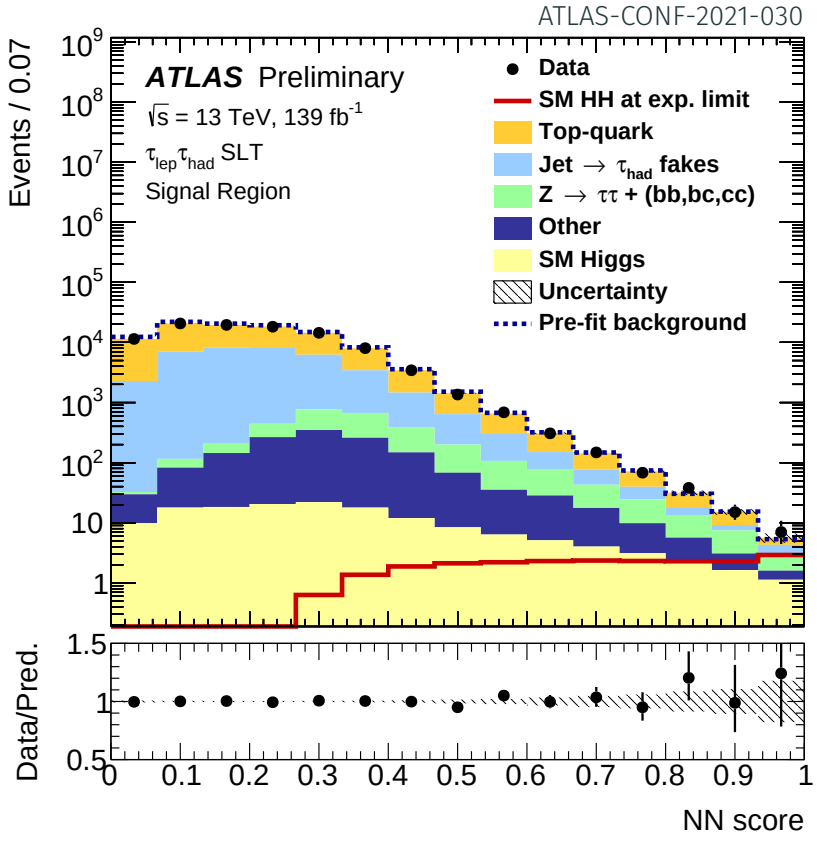

- Signal / background classifiers provide discriminant for likelihood fit

  $\tau_{\text{had}}\tau_{\text{had}}$: Boosted Decision Trees $\tau_{\text{lep}}\tau_{\text{had}}$: Neural Networks

- Trained on signal vs. all backgrounds using high-level variables:
  E.g. m_{HH}, m_{bb}, $m_{\tau\tau}^{\text{MMC}}$, $\Delta R(\tau,\tau)$, ...

Signal Extraction: Resonant Higgs Pair Production

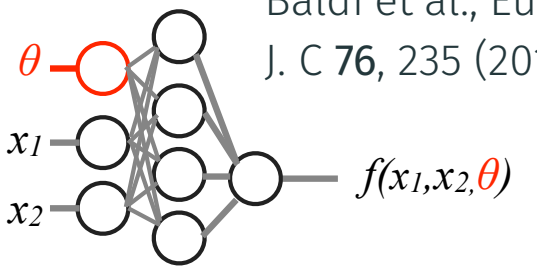

Baldi et al., Eur. Phys. J. C **76**, 235 (2016).

- Approach similar to non-resonant case
- Parametrized neural networks (PNN) used as discriminant
  - Parametrized in mass of scalar ($\theta = m_X$)
- Provides single classifier (per channel) for all considered m_X

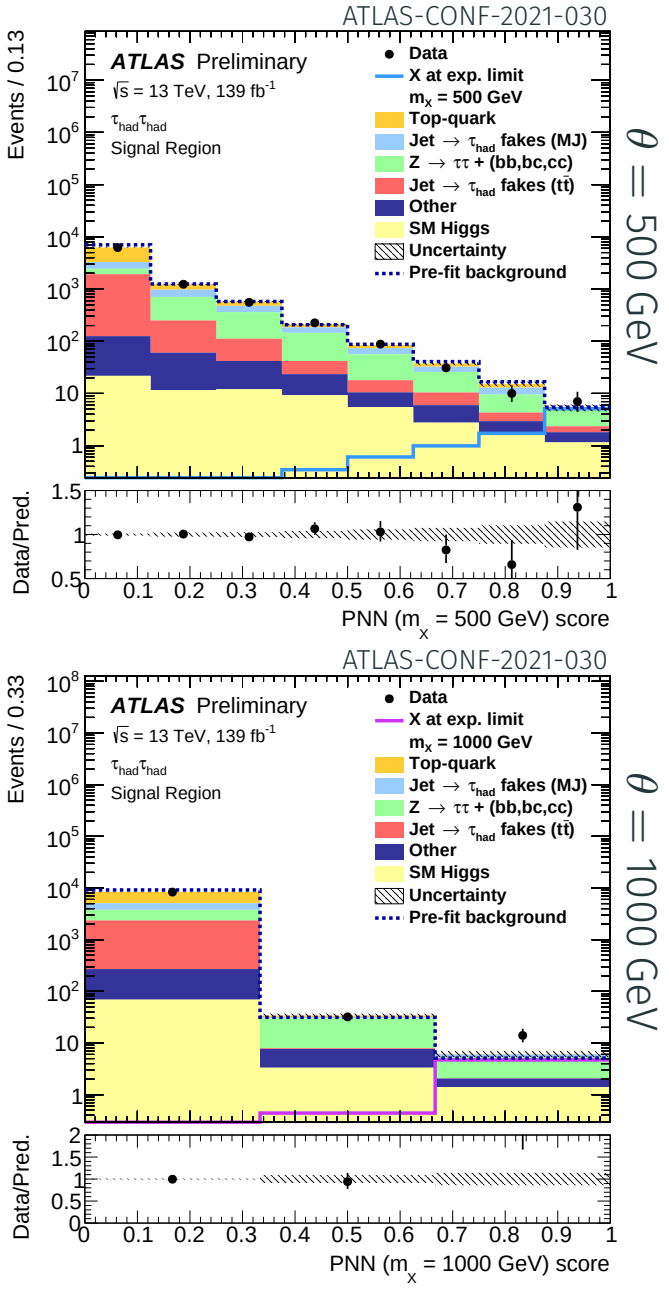

Uncertainties

- Uncertainty on signal strength statistically dominated
- Leading systematic sources (non-res. *HH*):
  - MC statistics
  - Top / Single Higgs modelling

Search for $X \to HH$:

- Similar picture
- Depending on m_X: Fake-τ_{had}, Z+jets, signal modeling up to 30 %

Relative uncertainty explained by source:

Uncertainty source	Non-resonant HH
Data statistical	81%
Systematic	59%
$t\bar{t}$ and Z + HF normalisations	4%
MC statistical	28%
Experimental	
Jet and $E_{\text{T}}^{\text{miss}}$	7%
b-jet tagging	3%
$\tau_{\text{had-vis}}$	5%
Electrons and muons	2%
Luminosity and pileup	3%
Theoretical and modelling	
Fake-$\tau_{\text{had-vis}}$	9%
Top-quark	24%
$Z(\to \tau\tau)$ + HF	9%
Single Higgs boson	29%
Other backgrounds	3%
Signal	5%

ATLAS-CONF-2021-030

$$\frac{\sqrt{\Delta\mu_{\text{tot}}^2 - \Delta\mu_{\text{categ.-fixed}}^2}}{\Delta\mu_{\text{tot}}}$$

Results: Upper Limits on Cross Sections

$pp \to HH$ (non-resonant, SM)

ATL-PHYS-PUB-2021-031

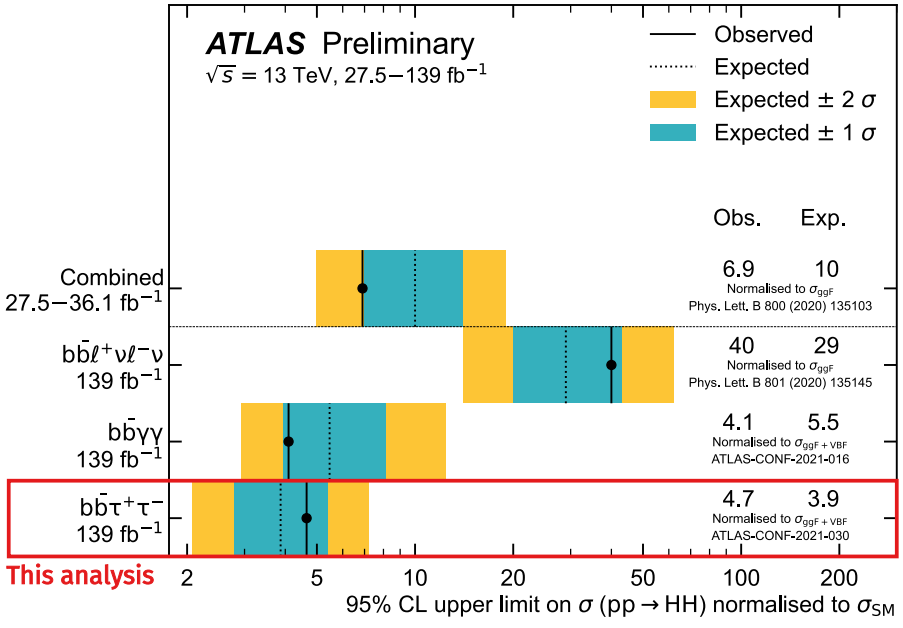

$pp \to X \to HH$ (resonant)

ATLAS-CONF-2021-030

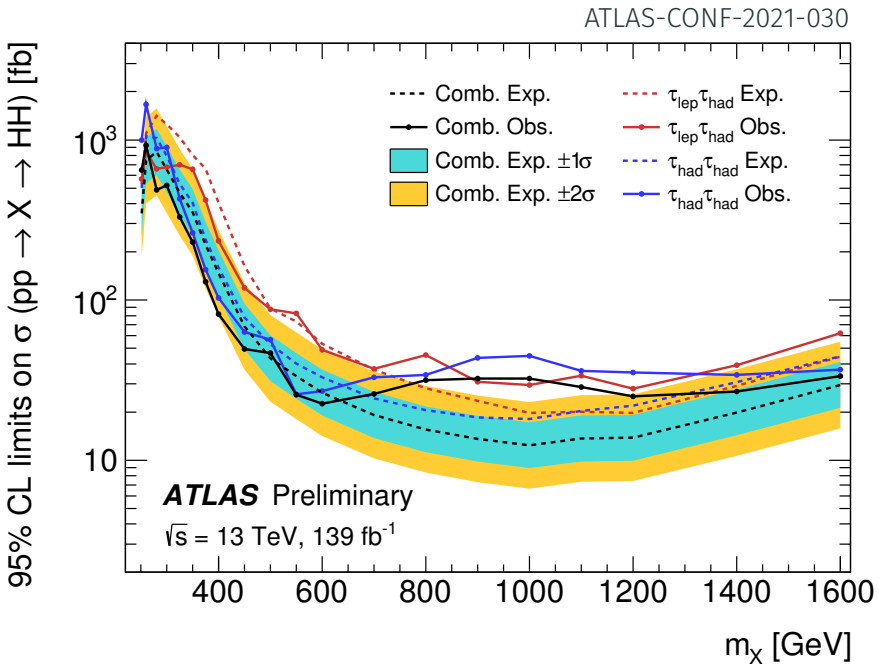

- Upper limit on $\sigma_{HH}^{\text{ggF+VBF}}$: obs. $4.7 \times \sigma_{\text{SM}}$ (exp. $3.9 \times \sigma_{\text{SM}}$)
  - Highest expected sensitivity to date

- Upper limits on $\sigma_{X \to HH}$ for narrow-width scalars ranging from approx. 20–10^3 fb
  - Largest excess at 1 TeV with local (global) significance of 3.0σ (2.0σ)

Reinterpretation: Anomalous Higgs Self-Coupling

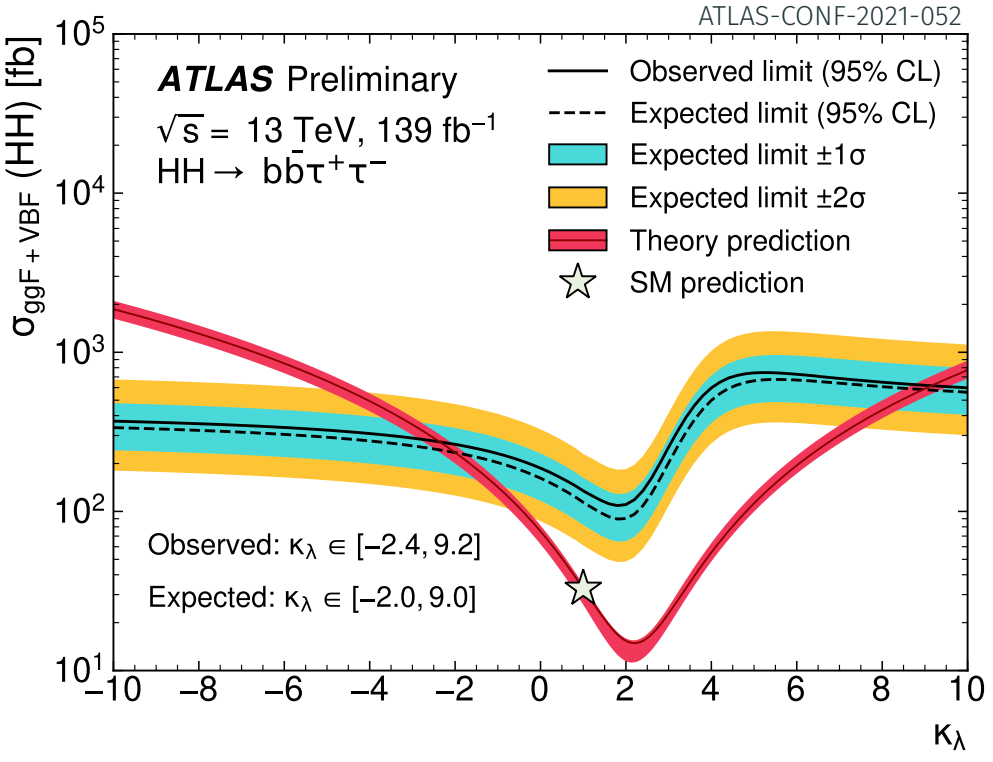

- Reinterpretation of non-res. *HH* search for anomalous values of the self-coupling modifier $\kappa_\lambda = \lambda_{HHH}/\lambda^{SM}_{HHH}$
- Comparable to ATLAS $b\bar{b}\gamma\gamma$ constraints on κ_λ (exp. $\kappa_\lambda \in [-2.4, 7.7]$)
  - Limited signal acceptance at low m_{HH} in $b\bar{b}\tau^+\tau^-$ detrimental in scenarios with a soft m_{HH} spectrum (e.g. large κ_λ)

Conclusion

ATLAS Combination with $b\bar{b}\gamma\gamma$ (139 fb^{-1}):

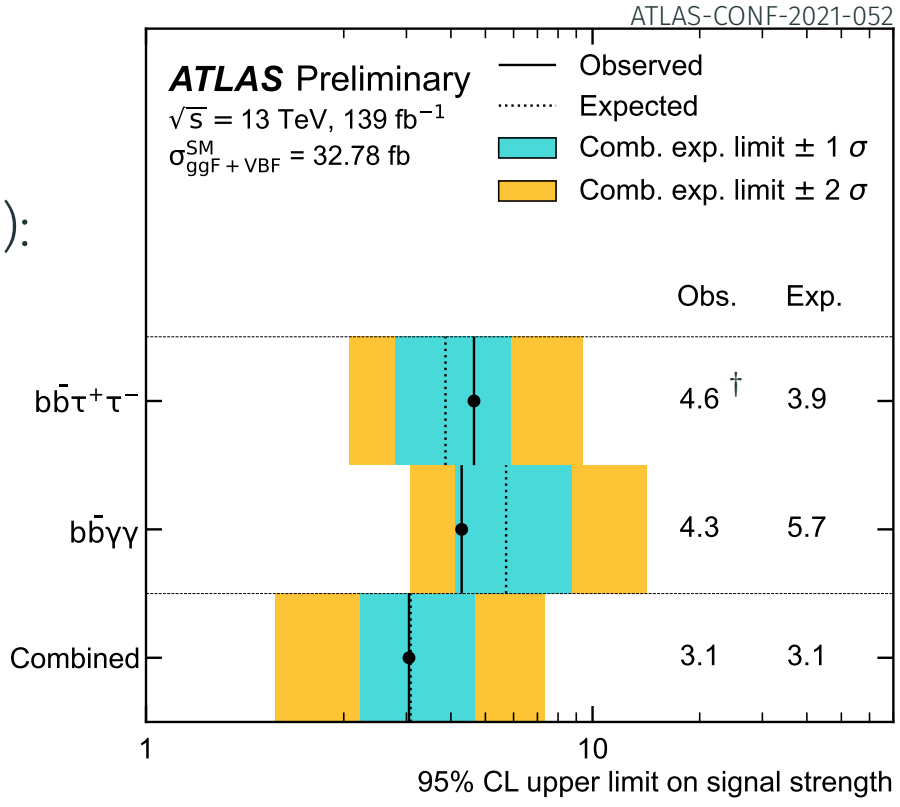

†: Difference to sl. 12: different m_H assumptions & small bugfix

- Far exceeding expectations based on luminosity scaling ($\approx$ factor two)

$\rightarrow$ Big parts due to large improvements in b-jet and $\tau_{\text{had-vis}}$ reconstruction & identification during Run 2 of the LHC

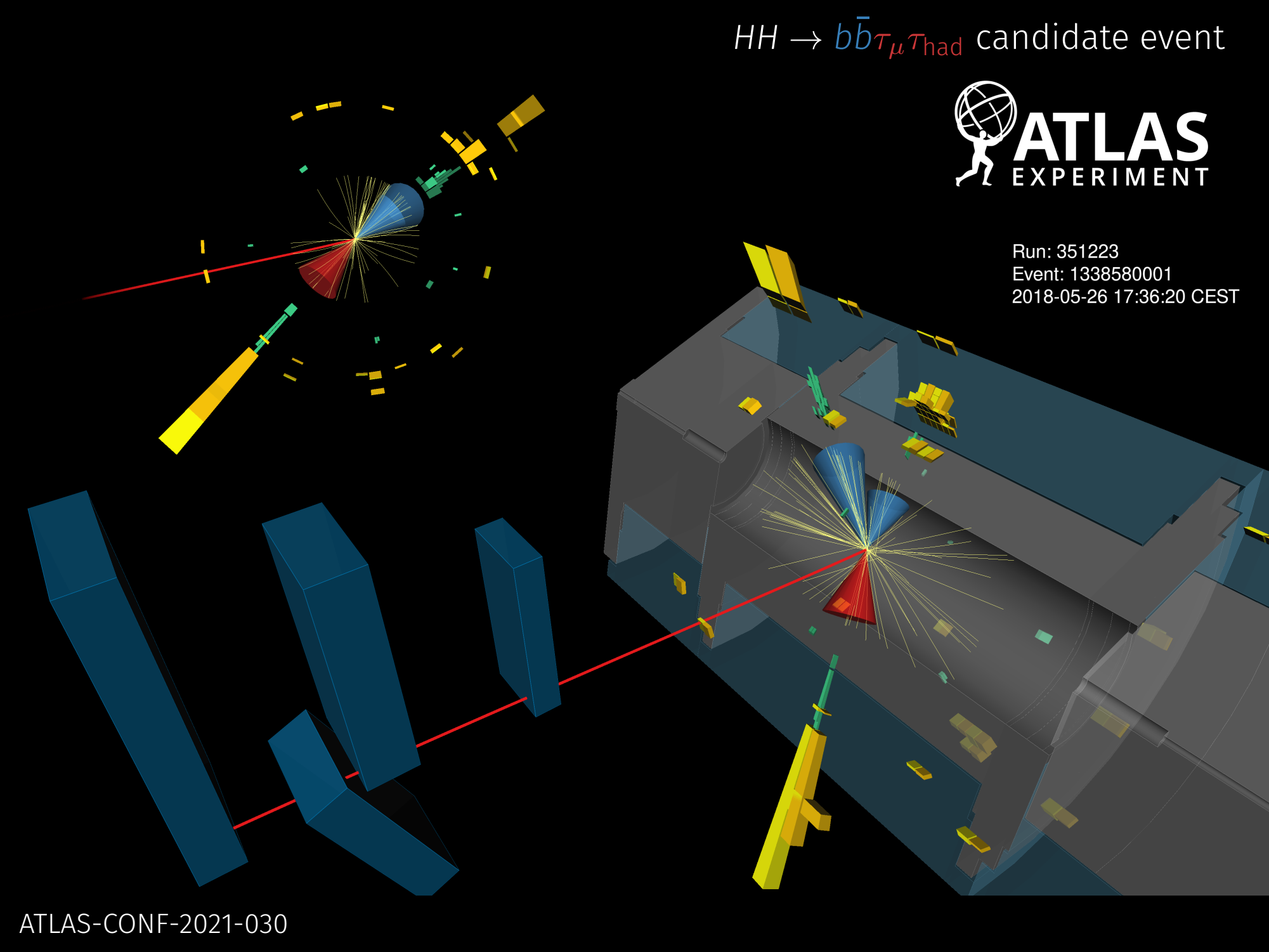
$HH \to b\bar{b}\tau_\mu\tau_{had}$ candidate event
ATLAS EXPERIMENT
Run: 351223
Event: 1338580001
2018-05-26 17:36:20 CEST
ATLAS-CONF-2021-030

$HH \to b\bar{b}\tau_{\text{had}}\tau_{\text{had}}$ candidate event

ATLAS EXPERIMENT

Run: 339535
Event: 996385095
2017-10-31 00:02:20 CEST

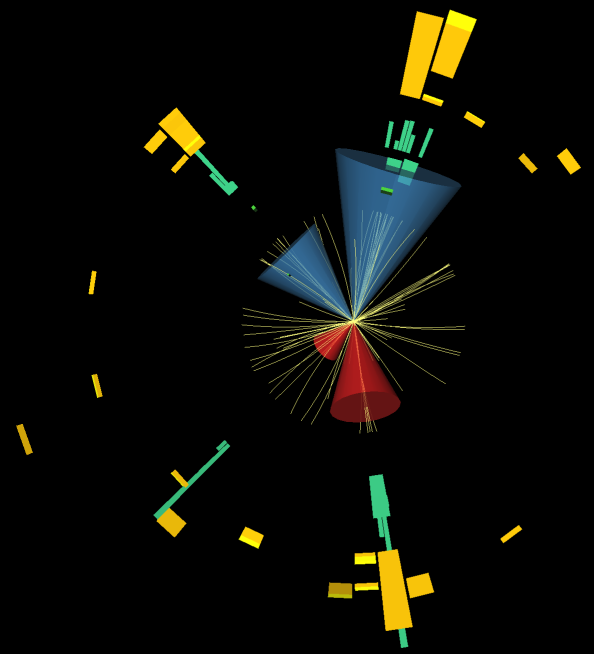

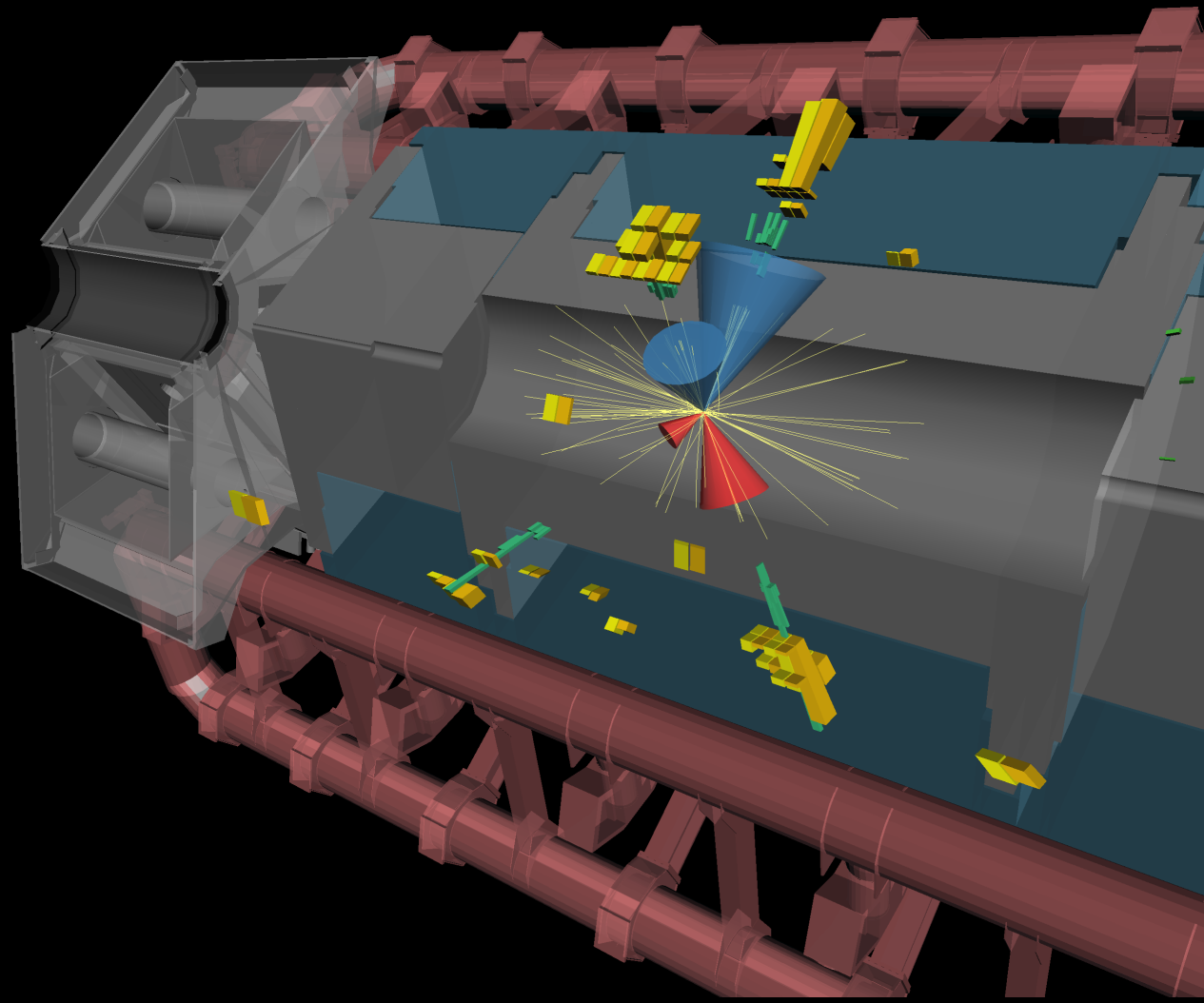

ATLAS-CONF-2021-030

Backup

Rebinning Algorithm

ATLAS-CONF-2021-030

The binning schemes for the MVA output distributions used in the likelihood fit were chosen to minimise the number of bins, while also maximising the retained expected sensitivity, and ensuring the stability of the fit and the validity of the asymptotic approximation. The binning schemes start from finely-binned histograms, and bins are iteratively merged beginning from the most signal-like MVA bins until the following channel-dependent criteria are fulfilled. In the $\tau_{\text{had}}\tau_{\text{had}}$ channel, the bins are required to satisfy $\sigma_b^{\text{MC}} < 0.5 f_s + 1\%$, where σ_b^{MC} is the relative MC statistical uncertainty in the background estimate and f_s is the fraction of signal in the bin. In the $\tau_{\text{lep}}\tau_{\text{had}}$ channel, the bins are required to satisfy $10 f_s + 5 f_b > 1$, where f_s and f_b are the fraction of signal and background in the bin, respectively. Bins in all channels are required to contain at least 5 expected background events to ensure that the asymptotic approximation is valid.

Selection

$\tau_{had}\tau_{had}$ category		$\tau_{lep}\tau_{had}$ categories	
STT	DTT	SLT	LTT
e/μ selection			
No loose e/μ with $p_T > 7$ GeV		Exactly one tight e or medium μ	
		$p_T^e > 25, 27$ GeV	18 GeV $< p_T^e <$ SLT cut
		$p_T^\mu > 21, 27$ GeV	15 GeV $< p_T^\mu <$ SLT cut
		$\lvert\eta^e\rvert < 2.47$, not $1.37 < \lvert\eta^e\rvert < 1.52$	
		$\lvert\eta^\mu\rvert < 2.7$	
$\tau_{had\text{-}vis}$ selection			
Two loose $\tau_{had\text{-}vis}$		One loose $\tau_{had\text{-}vis}$	
$\lvert\eta\rvert < 2.5$		$\lvert\eta\rvert < 2.3$	
$p_T > 100, 140, 180$ (25) GeV	$p_T > 40$ (30) GeV	$p_T > 20$ GeV	$p_T > 30$ GeV
Jet selection			
≥ 2 jets with $\lvert\eta\rvert < 2.5$			
$p_T > 45$ (20) GeV	Trigger dependent	$p_T > 45$ (20) GeV	Trigger dependent
Event-level selection			
Trigger requirements passed			
Collision vertex reconstructed			
$m_{\tau\tau}^{MMC} > 60$ GeV			
Opposite-sign electric charges of $e/\mu/\tau_{had\text{-}vis}$ and $\tau_{had\text{-}vis}$			
Exactly two b-tagged jets			
			$m_{bb} < 150$ GeV

ATLAS-CONF-2021-030

MVA Input Variables

Variable	$\tau_{\text{had}}\tau_{\text{had}}$	$\tau_{\text{lep}}\tau_{\text{had}}$ SLT	$\tau_{\text{lep}}\tau_{\text{had}}$ LTT
m_{HH}	✓	✓	✓
$m_{\tau\tau}^{\text{MMC}}$	✓	✓	✓
m_{bb}	✓	✓	✓
$\Delta R(\tau,\tau)$	✓	✓	✓
$\Delta R(b,b)$	✓	✓	
$\Delta p_{\text{T}}(\ell,\tau)$		✓	✓
Sub-leading b-tagged jet p_{T}		✓	
m_{T}^{W}		✓	
$E_{\text{T}}^{\text{miss}}$		✓	
$\mathbf{p}_{\text{T}}^{\text{miss}}$ ϕ centrality		✓	
$\Delta\phi(\tau\tau,bb)$		✓	
$\Delta\phi(\ell,\mathbf{p}_{\text{T}}^{\text{miss}})$			✓
$\Delta\phi(\ell\tau,\mathbf{p}_{\text{T}}^{\text{miss}})$			✓
S_{T}			✓

ATLAS-CONF-2021-030

Uncertainty Breakdown

Table 4: Breakdown of the relative contributions to the uncertainty in the extracted signal cross-sections, as determined in the likelihood fit to data. These are obtained by fixing the relevant nuisance parameters in the likelihood fit, and subtracting the obtained uncertainty on the fitted signal cross-sections in quadrature from the total uncertainty, and then dividing the result by the total uncertainty. The sum in quadrature of the individual components differs from the total uncertainty due to correlations between the groups of uncertainties.

Uncertainty source	Non-resonant HH	Resonant $X \to HH$		
		300 GeV	500 GeV	1000 GeV
Data statistical	81%	75%	89%	88%
Systematic	59%	66%	46%	48%
$t\bar{t}$ and Z + HF normalisations	4%	15%	3%	3%
MC statistical	28%	44%	33%	18%
Experimental				
Jet and $E_{\mathrm{T}}^{\mathrm{miss}}$	7%	28%	5%	3%
b-jet tagging	3%	6%	3%	3%
$\tau_{\text{had-vis}}$	5%	13%	3%	7%
Electrons and muons	2%	3%	2%	1%
Luminosity and pileup	3%	2%	2%	5%
Theoretical and modelling				
Fake-$\tau_{\text{had-vis}}$	9%	22%	8%	7%
Top-quark	24%	17%	15%	8%
$Z(\to \tau\tau)$ + HF	9%	17%	9%	15%
Single Higgs boson	29%	2%	15%	14%
Other backgrounds	3%	2%	5%	3%
Signal	5%	15%	13%	34%

ATLAS-CONF-2021-030

Additional Plots for SLT

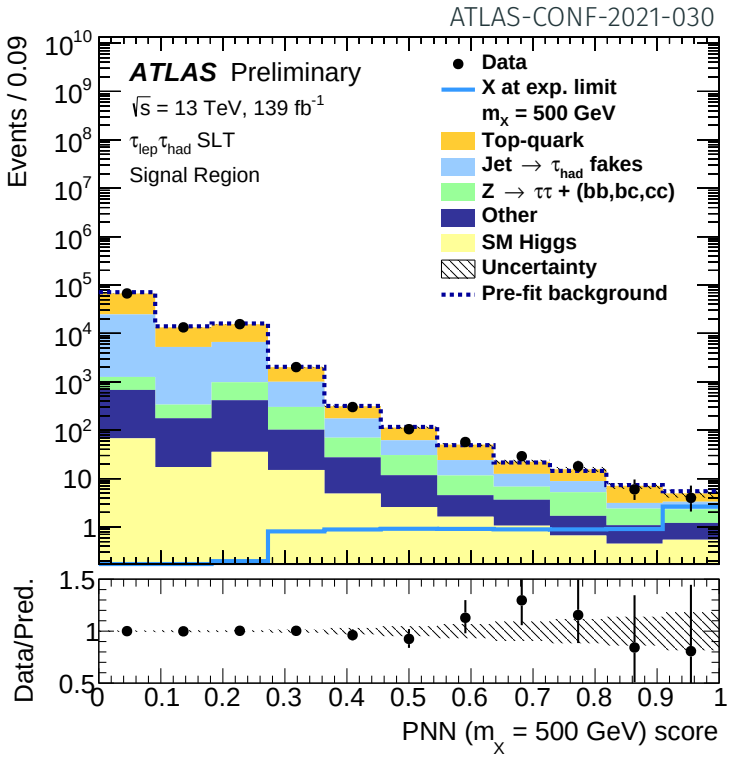

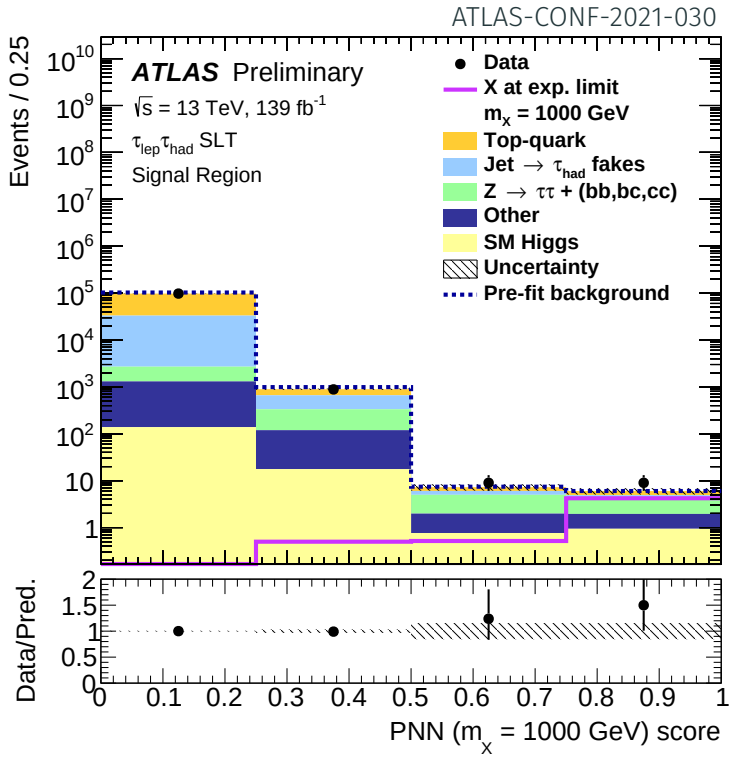

Additional Plots for LTT (1)

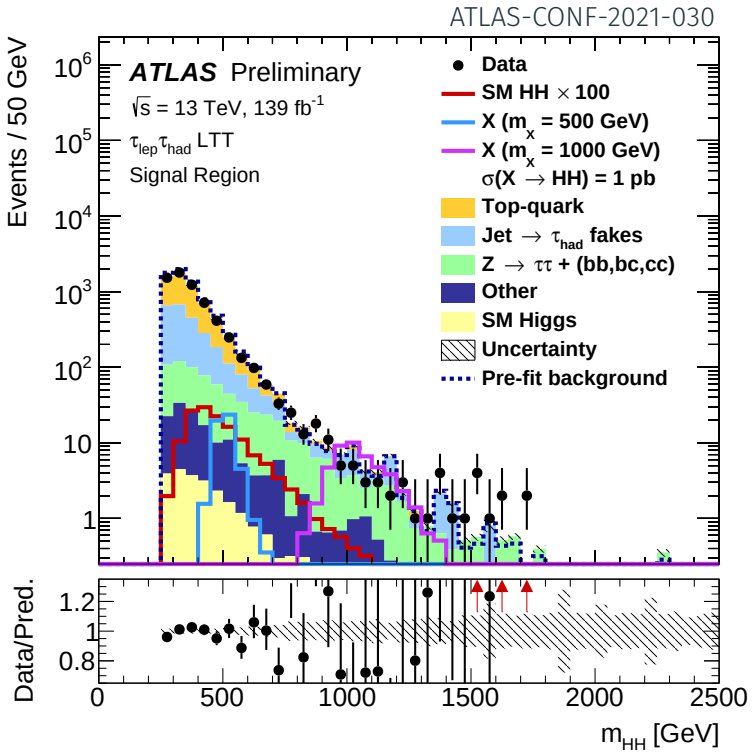

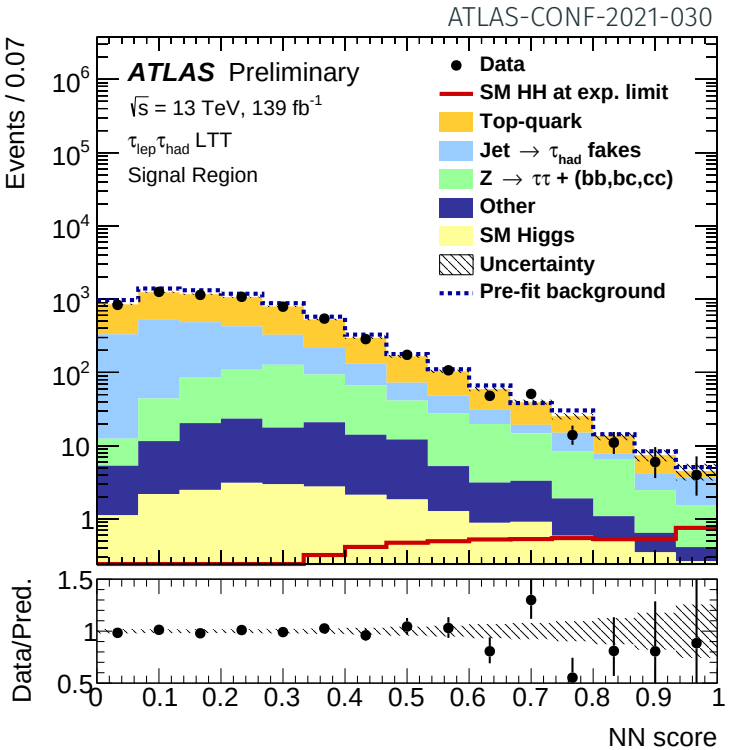

Additional Plots for LTT (2)

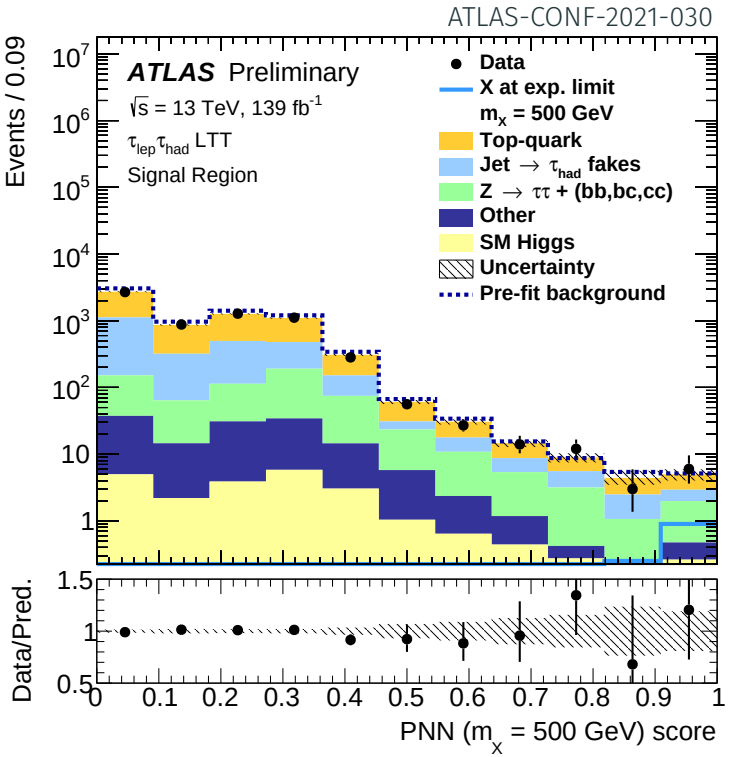

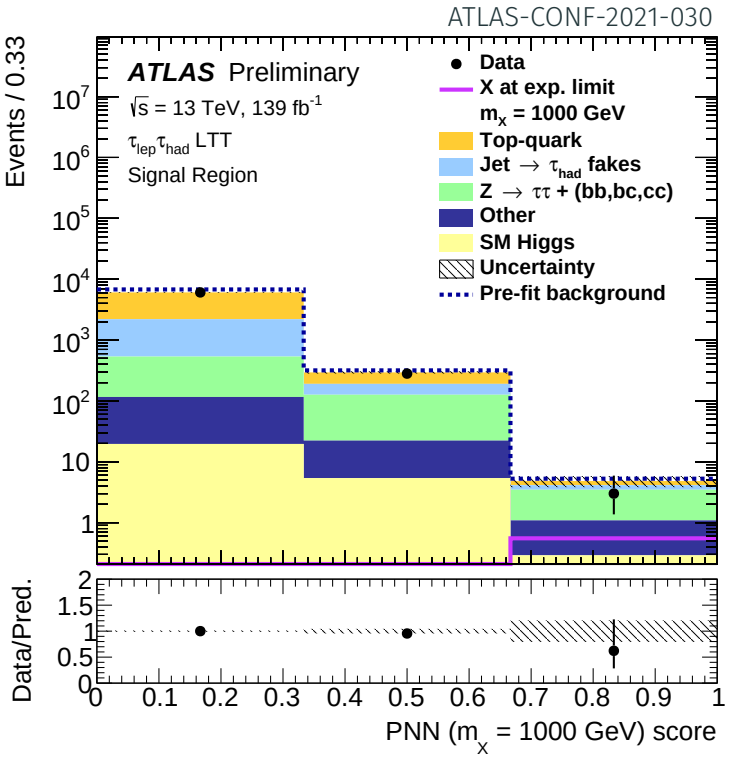

Non-Resonant HH Results

Table 5: Observed and expected upper limits at 95% CL on the cross-section of non-resonant HH production according to SM-like kinematics, and on the cross-section of non-resonant HH production divided by the SM prediction. The $\pm 1\,\sigma$ and $\pm 2\,\sigma$ variations around the expected limit are also shown.

		Observed	$-2\,\sigma$	$-1\,\sigma$	Expected	$+1\,\sigma$	$+2\,\sigma$
$\tau_{\text{had}}\tau_{\text{had}}$	$\sigma_{\text{ggF+VBF}}$ [fb]	145	70.5	94.6	131	183	245
	$\sigma_{\text{ggF+VBF}}/\sigma^{\text{SM}}_{\text{ggF+VBF}}$	4.95	2.38	3.19	4.43	6.17	8.27
$\tau_{\text{lep}}\tau_{\text{had}}$	$\sigma_{\text{ggF+VBF}}$ [fb]	265	124	167	231	322	432
	$\sigma_{\text{ggF+VBF}}/\sigma^{\text{SM}}_{\text{ggF+VBF}}$	9.16	4.22	5.66	7.86	10.9	14.7
Combined	$\sigma_{\text{ggF+VBF}}$ [fb]	135	61.3	82.3	114	159	213
	$\sigma_{\text{ggF+VBF}}/\sigma^{\text{SM}}_{\text{ggF+VBF}}$	4.65	2.08	2.79	3.87	5.39	7.22

ATLAS-CONF-2021-030

Background Estimation

Combined Fake Factor Method ($\tau_{\text{lep}}\tau_{\text{had}}$)

ATLAS-CONF-2021-030

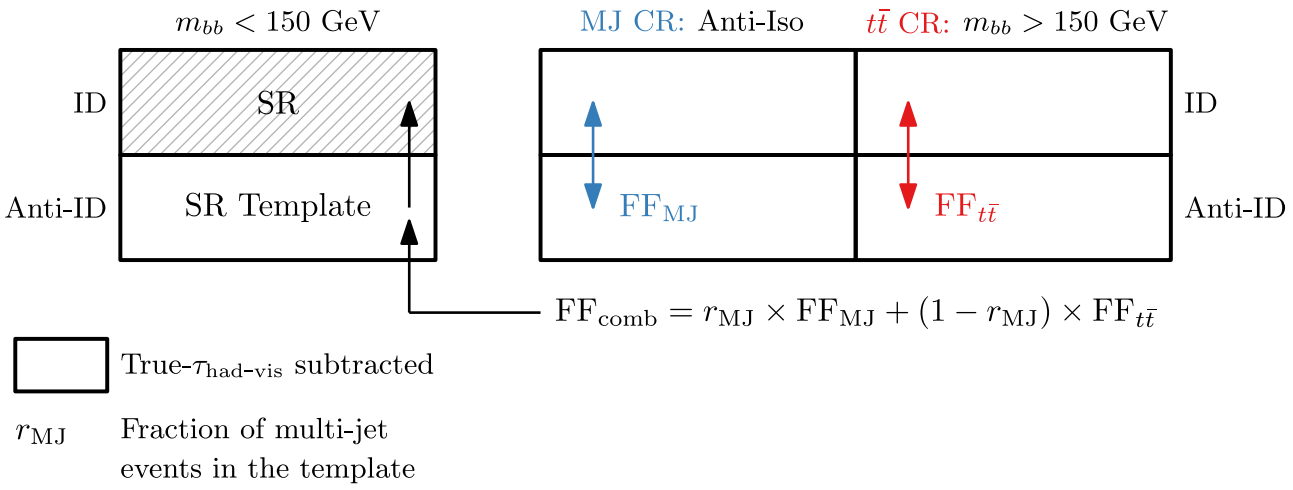

Figure 4: Schematic depiction of the combined fake-factor method used to estimate multi-jet and $t\bar{t}$ backgrounds with fake-$\tau_{\text{had-vis}}$ in the $\tau_{\text{lep}}\tau_{\text{had}}$ channel. Backgrounds which are not from events with fake-$\tau_{\text{had-vis}}$ originating from jets are estimated from simulation and are subtracted from data in all control regions. Events in which an electron or a muon is misidentified as a $\tau_{\text{had-vis}}$ are also subtracted, but their contribution is very small. Both sources are indicated by "True-$\tau_{\text{had-vis}}$ subtracted" in the legend.

Fake Factor Method ($\tau_{\text{had}}\tau_{\text{had}}$)

ATLAS-CONF-2021-030

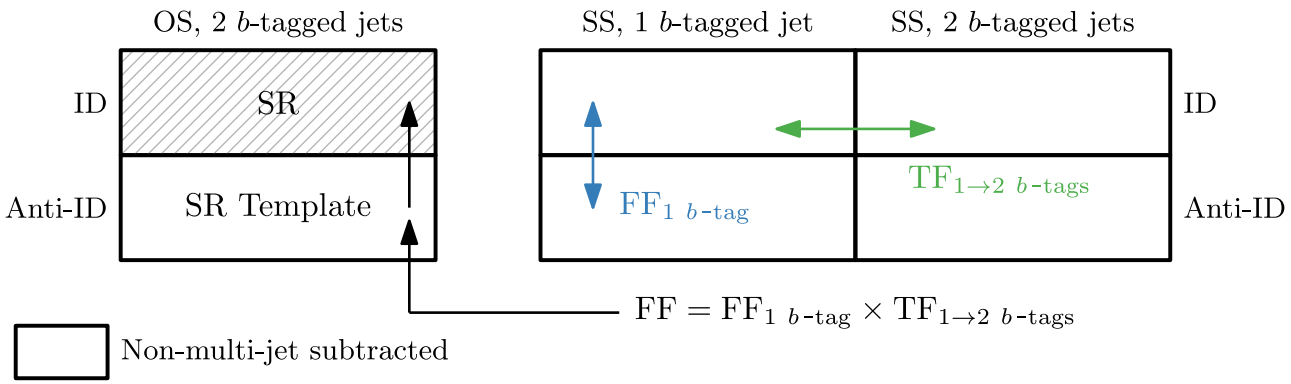

Figure 5: Schematic depiction of the combined fake-factor method to estimate the multi-jet background with fake-$\tau_{\text{had-vis}}$ in the $\tau_{\text{had}}\tau_{\text{had}}$ channel. Backgrounds with true-$\tau_{\text{had-vis}}$ that are not from multi-jet events are simulated and subtracted from data in all the control regions. This is indicated by "Non-multi-jet subtracted" in the legend.

$t\bar{t}$ Misidentification Efficiency ($\tau_{\text{had}}\tau_{\text{had}}$)

ATLAS-CONF-2021-030

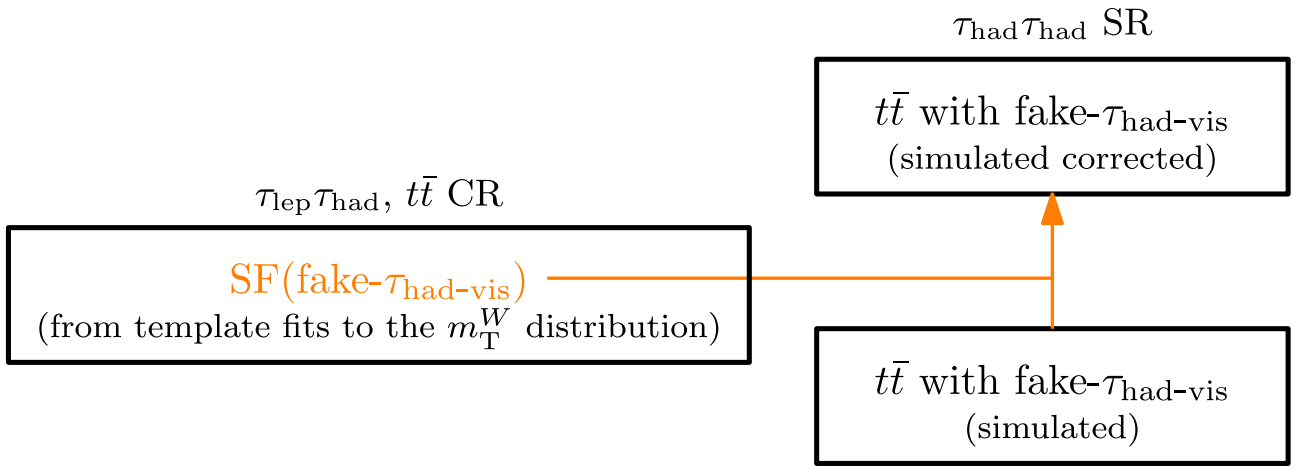

Figure 6: Schematic depiction of the fake-$\tau_{\text{had-vis}}$ scale-factor method to estimate the $t\bar{t}$ background with fake-$\tau_{\text{had-vis}}$ in the $\tau_{\text{had}}\tau_{\text{had}}$ channel.

p_0-Value Scan

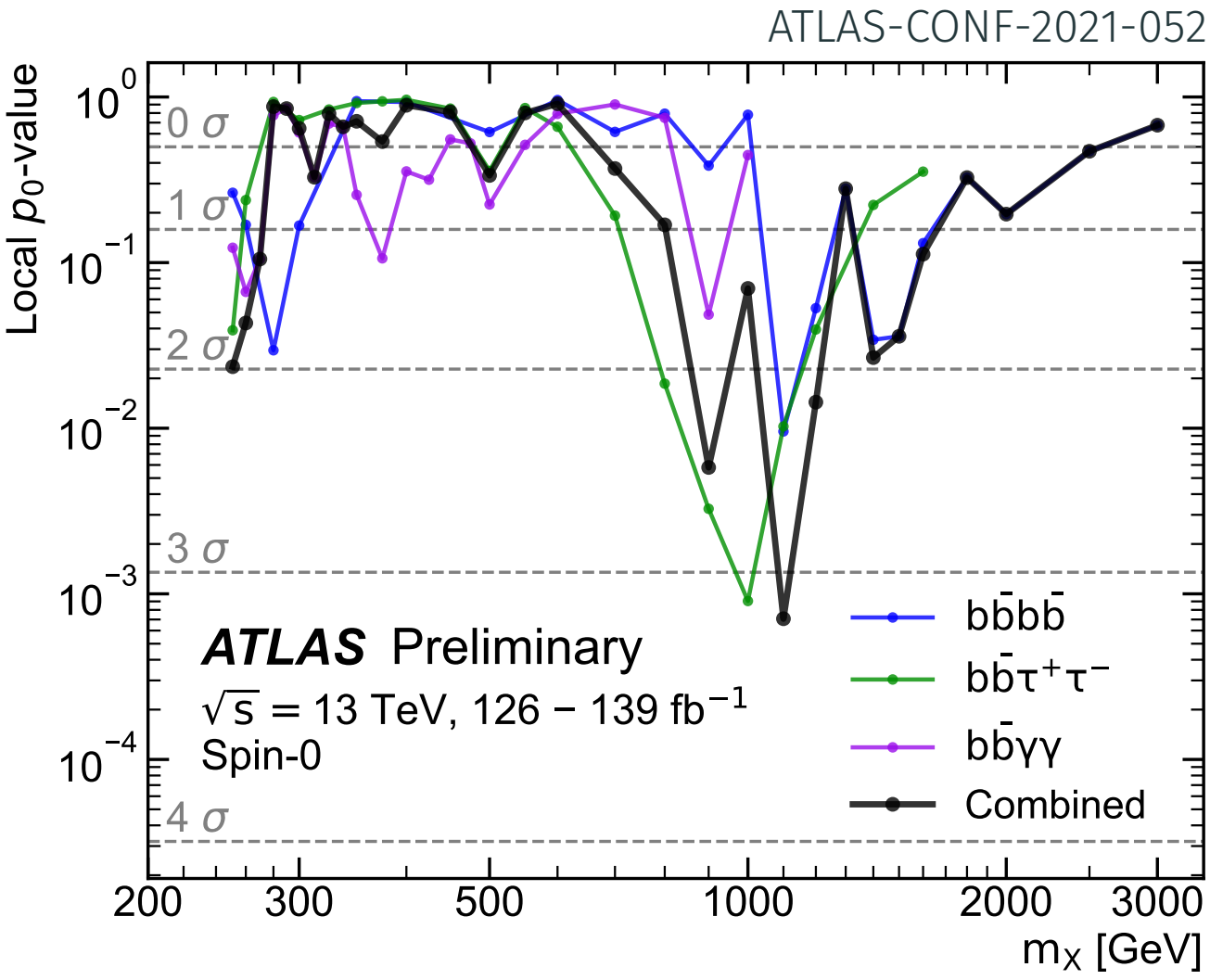

Acceptance vs. κ_λ

ATLAS-CONF-2021-052